Journal of Magnetic Resonance **154,** 6–14 (2002)
doi:10.1006/jmre.2001.2459, available online at http://www.idealibrary.com on IDEAL®

Kinetic Measurements Using EPR Imaging with a Modulated Field Gradient

Thomas Herrling,* Jürgen Fuchs,† and Norbert Groth‡

*FOM Institute, University of Applied Science and Technology, TFH Berlin, Germany; †Department of Dermatology, University Clinic Frankfurt, Frankfurt, Germany; and ‡Privatinstitute Galenus Berlin, Berlin, Germany

Received January 16, 2001; revised October 24, 2001

EPR imaging with modulated field gradient was applied for the investigation of fast diffusion processes. Three different imaging methods are possible: spectral–temporal, spatio–temporal, and spectral–spatial imaging. The time resolution is on the order of seconds and the spatial resolution is in the micrometer region. The efficiency of this imaging technique is demonstrated for the penetration of the spin probe Tempol in the skin of hairless mice biopsies. The skin is normally protected against the penetration of water soluble substances by the horny layer, a resistive thin lipophilic layer. Overcoming this horny layer for water soluble ingredients is one of the main practical problems for the topical application of pharmaceutics which could be investigated by EPR imaging. Different images represent the penetration behavior of the water soluble Tempol in the skin after treatment with the penetration enhancer DMSO (Dimethylsulfoxide) and after removing the horny layer.

Key Words: **EPR imaging; modulated field gradient; diffusion process; penetration enhancement.**

INTRODUCTION

The study of diffusion processes especially in biology and medicine is often related to time dependencies on the order of minutes or seconds. The application of spectral–spatial EPRI (*1, 2*) can give information about the micro- and macromolecular environment of the sample using paramagnetic spin probes. The spatial tomogram gives information about the macromolecular structure of the sample and the EPR spectrum gives information about the micromolecular structure caused by the mobility of the spin probe. Spectral–spatial imaging is a well-known method for measuring diffusion profiles. Two methods of spectral–spatial imaging exist up to now. The first frequently used method requires, for the generation of a 2D spectral–spatial image, a sequence of scans measured with numerous field gradients, normally 32 or 64 different gradient values. The image reconstruction can be performed only after the last scan. The recording time of such 2D spectral–spatial images requires about 7 to 30 minutes (*3–7*), which is too long for measuring consecutive images reflecting an acceptable diffusion profile. Therefore the investigation of fast diffusion processes using this method is not possible. Time dependent diffusion processes were measured by Ohno *et al*. (*8*) on irradiated polymers with time intervals of 4, 120, and 700 h. Schlick *et al*. (*9*) measured diffusion processes of Tempol in hydrogels with time intervals from 1.4 to 31 h.

The second method uses a modulated field gradient (*10*). Together with a simultaneous superimposed field scan, a row of localized spectra are measured by shifting the local plane (zero plane of the modulated field gradient) and a spectral-spatial image is measured. This method is called Modulated Gradient with Simultaneous Superimposed Field Scan (MOSS) (*11, 12*). Using this method, numerous diffusion profiles of spin probes in skin biopsies were measured by Fuchs *et al*. (*13–15*). The acquisition time for the 2D images was between 2 and 4 minutes for a 64×64 image matrix and a 128×128 matrix, respectively. Mäder *et al*. (*16*) used this method for measuring the diffusion of water in polymers containing a homogenous distribution of Tempol. The observed diffusion time varied between 1 and 120 h. Using the modulated field gradient Pali *et al*. (*17*) measured the lipid lateral diffusion of spin-labeled stearic acid in oriented and unoriented dimyristoyl phophatidylcholine multilayers and represented it in a 2D distribution image.

The use of EPR imaging for studying fast diffusion processes could increase the application of this method also for biological samples. The skin appears to be an attractive and effective approach for such measurements because of the importance of this organ system and its accessibility. The skin is an ideal object for EPR imaging because it is a biological organ with only one dimension which is interesting for diffusion and penetration processes. This dimension is the thickness of the skin. The thickness is smaller than 1 mm and the measurement of thin skin biopsies is conveniently possible in a normal X-band rectangular H_{102} cavity using a tissue cell. The penetration behavior of active ingredients in skin formulations has a relevant importance for pharmacology and cosmetics. EPR imaging is a method which was often used for the measurement of penetration profiles in organic and inorganic media. Several researchers (*18–25*) have measured the penetration profile of spin probes and labeled liposomes in skin biopsies by EPR tomography. The results of these measurements were 1D diffusion profiles of the skin.

1090-7807/02 $35.00

Transport properties of water-soluble low-molecular-weight compounds in the skin play an important role as ingredients in medical and also in cosmetic industry applications. The diffusion of substances into the skin is restricted by the horny layer of the skin (stratum corneum) consisting in a lipid rich layer from keratinocytes separated by intracellular lipids which are structured into multilamellar bilayers (*26, 27*). The physical and chemical properties of these lipids are thought to be of major importance in maintaining the barrier function of the skin. It is widely accepted that the permeability of the skin is controlled mainly by passive diffusion through the stratum corneum, the uppermost nonviable layer of the epidermis.

Using the skin model the versatility of the modulated field gradient technique should be demonstrated for kinetic measurements on membranes. The MOSS technique (*11, 12*) offers three possibilities for the measurement of diffusion processes in membranes which result in three different 2D images:

1. Localized spectral–temporal images $\mathrm{IM}(\mathbf{B}, t)_{\mathrm{ro}}$ represent a stack plot of EPR spectra of the region of interest, recorded at different time. These images can provide information about time dependent intensity and spectral changes in an observed plane $\mathbf{r}_{\mathrm{o}}$ which is characterized by the zero plane of the modulated field gradient.

2. Timed spectral–spatial images $\mathrm{IM}(\mathbf{B}, \mathbf{r})_{\mathrm{to}}$ are measured during a time interval Δt which is determined by the collection time and a completion time t_{o}. The collection time for 2D spectral–spatial images is normally on the order of some minutes which is too long for the investigation of fast diffusion processes. But these images supply both a distribution profile of the spin probe and the spectral distribution of the diffusant in the different planes of the sample.

3. Field fixed spatio–temporal images $\mathrm{IM}(\mathbf{r}, t)_{B\mathrm{o}}$ give time dependent spatial information of the diffusion process provided that the line shape of the paramagnetic center remains unchanged.

By the application of these three imaging procedures it should be possible to describe fast diffusion processes in different samples like for instance in the skin.

EXPERIMENTAL

The main objective of this study was the exploration of the potential of the 2D MOSS EPRI as a method for measuring of diffusion kinetics. As a model sample we used the skin which is characterized by different layers with different diffusion properties. The skin reacts like a membrane which protects the body against external hazards. The main barrier especially for hydrophilic substances is the upper layer, the horny layer (stratum corneum). So we have tested the diffusion behavior of the water solved spin probe Tempol.

The diffusion characteristic of Tempol in the skin was demonstrated for the untreated and treated skin. Because the horny layer is the main barrier for diffusion we have tried to influence this upper layer. The horny layer was changed in a chemical and a physical way. The chemical treatment of the horny layer was performed with the known penetration enhancer DMSO (Dimethylsulfoxide) (*28, 29*). The physical influence on the horny layer was characterized by removing this layer with tape stripping which is also a known method for removing the horny layer from the skin.

Materials

All chemicals like 4-Hydroxy-2,2,6,6-tetramethyl-piperidine-1-oxyl (Tempol), Dimethylsulfoxide (DMSO), and N-ethyl-maleimide (NEM) were purchased from Sigma (Munich).

Euthymic, hairless mice (SKH1) were purchased from Charles River Wiga GmbH (Sulzfeld) After sacrificing the animals, 6-mm punch biopsies were cut from the back of the animals. The total thickness of the skin varied between 400 and 600 μm depending on the age of the animals (*15–24* weeks). Epidermal thickness at the back of the animals was about 30 μm and the thickness of the horny layer was about 10 μm. For the treated samples, 10 min before cutting the biopsy the back of the mouse was treated with a DMSO solution (30% DMSO in water) or the horny layer was removed by the tape stripping method. Tape stripping is a frequently used method in the fields of skin pharmacology and stratum corneum (horny layer) research. By applying and removing adhesive tapes onto the skin it is possible to subsequently remove the stratum corneum layer by layer from the underlying epidermis. Samples of the murine stratum corneum were obtained by tape stripping the skin with pieces of adhesive tape (Supreme Brand, Sekisui TA, Garden Grove, CA). The horny layer was stripped 10 times.

To prevent a rapid nitroxide reduction caused by the viability of the skin, all biopsies were stored for 10 min in a 50-mM solution of NEM. NEM readily penetrates into skin and reacts with protein and non protein thiol groups thereby blocking nitroxide reducing activity in epidermis and dermis.

Imaging System

The imaging system consists of an X-band EPR spectrometer ERS 221 (ZWG) and an accessory unit for EPR tomography ZZG 1 (ZWG) and is represented schematically in Fig. 1. The experimental arrangement was fully described in (*15*). The spectrometer and tomography settings are noted in Table 1. Contrary to *in vivo* EPR spectroscopy on human forearm (*15, 32*) which was performed at lower S-band (3 GHz) microwave frequency EPR imaging of skin requires a higher sensitivity which is given by X-band (9.5 GHz) microwave frequency and using a rectangular H_{102} cavity with a special tissue cell. The penetration depth of microwave frequencies of the X-band range is $\delta < 0.5$ mm in aqueous biological samples which is sufficient for skin biopsies of hairless mice.

The spatial scanning direction $\mathbf{r}$ and the magnetic field gradient $\mathrm{grad}_{\mathrm{r}}\mathbf{B}$ are oriented parallel to the z axis (axis of the $\mathbf{B}_{\mathrm{o}}$-field).

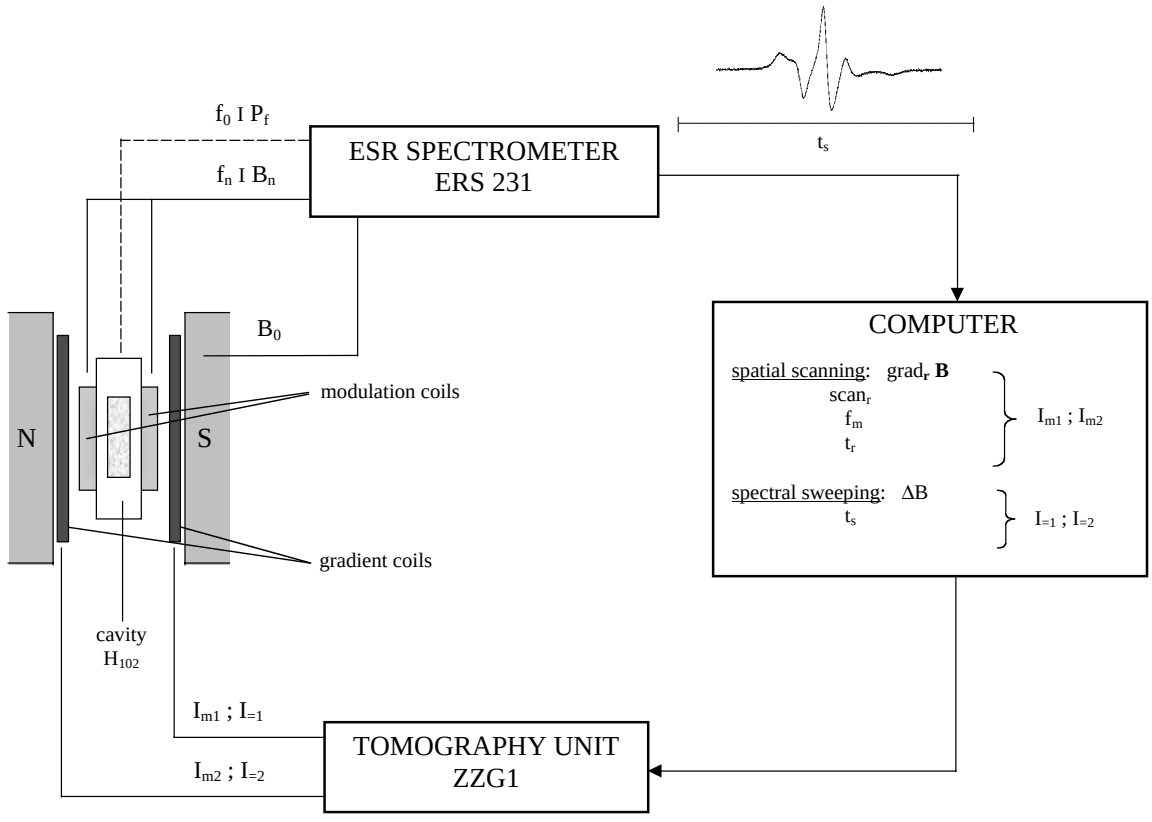

FIG. 1. The experimental arrangement for EPR imaging consists of a modified X-band ($f_0 = 9.5$ GHz) EPR spectrometer ERS 231 (ZWG-Berlin) including an electromagnet with a wide pole gap of 100 mm. The data recording for image reconstruction and the controlling of the imaging process is performed by a computer which is connected to the EPR spectrometer and the tomography unit ZZG1 (ZWG-Berlin). The data of the spatial scanning like the field gradient $\mathrm{grad_r}\mathbf{B}$, the spatial scan $s_\mathbf{r}$, the scan time t_r, and the modulation frequency of the field gradient $\mathbf{f}_\mathrm{m}$ were fed into the computer to calculate the amplitudes of the alternating current $I_{\mathrm{m}1}$ and $I_{\mathrm{m}2}$ for the two gradient coils. The spectral sweeping is characterized by the field sweep ΔB and the sweep time t_B which results in the superimposed direct currents $I_{=1} = I_{=2}$ for the two gradient coils. The detailed experimental data are given in Table 1.

The surface of the skin biopsy has to be oriented perpendicular to the z axis. This orientation enables the measurement of the penetration of the spin probe into the skin. For most practical applications only one direction of penetration is of interest: from the upper horny layer to the lower dermis.

The cover plate of the tissue cell contains a cylindrical cavity with a diameter of 4 mm and a depth of 0.5 mm filled with a microemulsion containing the spin probe Tempol in a final concentration of 1 mM. The spin probe was dissolved in a microemulsion consisting of 17.25% Tween 80, 5.175% dodecanol, 5.175% cera perliquida, 22.4% propylenglycol, and 50% water. The microemulsion is a pharmaceutical carrier system consisting of hydrophilic and hydrophobic components and a surfactant to decrease the surface tension of the hydrophobic component. To prevent line broadening effects of the spin probe reservoir we chose low spin probe concentrations. Immediately after connecting the basis plate, which contains the skin biopsy, with the cover plate the tissue cell was fixed in the microwave cavity and the first measurement was started after 1 min exactly. A correct mounting of the tissue cell was achieved if a maximum signal amplitude was seen on the screen of the spectrometer. The sample configuration with the orientation of the skin biopsy and the spin probe reservoir is shown in Fig. 2.

Measurement

All measurements of EPR imaging were performed by using the second derivative of the spectrum. For the conventional EPR spectroscopy the signal intensity of the second derivative is smaller than for the first derivative. Using the modulated field gradient method the spatial resolution of the images is higher for the second derivative (*11*) and a smaller field gradient is necessary to get the same spatial resolution like for the first derivative. The smaller signal intensity of the second derivative is compensated by a higher spatial resolution. This given fact is obviously if we compare the signal intensity A (*30, 31*) with the spatial resolution $\Delta\mathbf{r}$ (*10*) of the first $^1(\,)$ and second derivative $^2(\,)$ of a Lorentzian line:

$$^1A/^2A = 1.0/0.7 = 1.4; \quad ^1\Delta r/^2\Delta r = 0.66/0.46 = 1.4.$$

TABLE 1
Settings of the EPR Spectrometer ERS 221 and the Imaging Unit ZZG1

Spectrometer Settings	
Magnetic field	$B_0 = 0.33$ T
Microwave frequency	$f_0 = 9.5$ GHz (X-band)
Microwave power	$P_{fo} = 50$ mW
Modulation frequency (second derivative)	$f_n = 50$ kHz
Modulation amplitude	$B_n = 0.15$ mT
Time constant	$\tau = 20$ ms
Tomography Settings	
Field gradient	$\text{grad}_r\mathbf{B} = 5.2$ T/m
Gradient direction	z (parallel to $\mathbf{B}_0$)
Modulation frequency (cosine)	$f_m = 70$ Hz (180 Hz)
Spatial scan	$r = 3.0$ mm
Scan time	$t_r = 4$ s
Spectral sweep	$\Delta B = 10$ mT
Sweep time	$t_B = 4$ s
Image matrix	128×128 points
Spatial resolution (theoretical)	$\Delta r_c = 0.8\,\Delta B_{pp}/\text{grad}_r\mathbf{B}$ (Lorentzian line)
Achieved resolution	for $\Delta B_{pp} = 0.12$ mT $\text{grad}_r\mathbf{B} = 5.2$ T/m $\Delta r_c = 23\,\mu$m
Point resolution	$\Delta p = r/128$ points = 3.0 mm/128 $= 23\,\mu$m

Comparing the spatial resolutions of the MOSS technique ${}^2\Delta r_c$ (cosine modulation) and the method using a series of different stationary field gradients Δr_s we get

$$\Delta r_s/{}^2\Delta r_c = 1.0/0.46 = 2.17.$$

This ratio means a twofold higher spatial resolution for the MOSS imaging technique assuming the same maximum field gradient for both methods. Of course this higher spatial resolution is combined with a lower signal intensity of the MOSS images.

For the measurement of the MOSS images we chose a magnetic field gradient which was determined by the spatial scan $s_r = 3000\ \mu$m and the number of the pixel points of the image matrix $n_p^2 = 128 \times 128$. The number of $n_p = 128$ pixel for a spatial scan allows the measurement of a point resolution:

$$\Delta p = s_r/n_p = 3000\ \mu\text{m}/128 \text{ points} = 23.4\ \mu\text{m}.$$

The realization of this point resolution needs a field gradient of

$$\text{grad}_r\mathbf{B} = 0.46\,\Delta B_{1/2}/{}^2\Delta r_c = 0.46\,\sqrt{3}\,\Delta B_{pp}/{}^2\Delta r_c \quad \text{with}$$

$$\Delta p = {}^2\Delta r_c \quad \text{and} \quad \Delta B_{pp} = 0.15 \text{ mT} \quad \text{follows}$$

$$\text{grad}_r\mathbf{B} = 0.8 \cdot 0.15 \text{ mT}/23.4\,\mu\text{m} = 0.12\,\text{mT}/23.4\,\mu\text{m} = 5.13\,\text{T/m}.$$

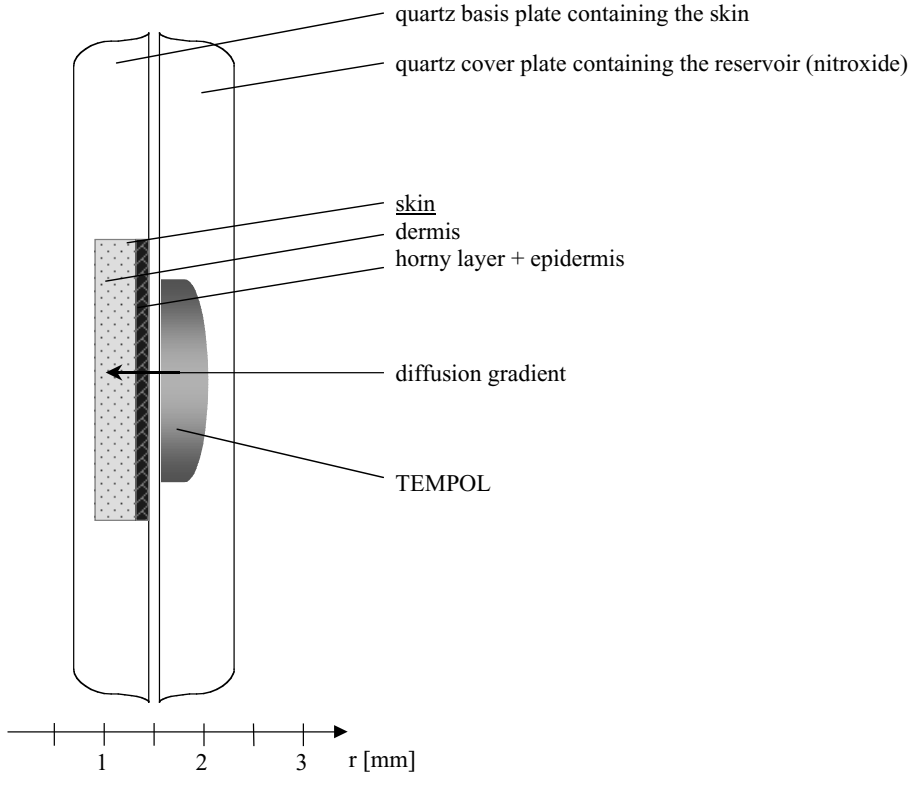

FIG. 2. Schematic representation of the sample configuration consisting of two quartz plates with a recess for the skin biopsy and a reservoir (diameter 4 mm) for the spin probe Tempol. The tissue cell with the skin biopsy (diameter 6 mm) is oriented perpendicular to the z axis (direction of the magnetic field) in a rectangular H_{102} cavity. The scanning orientation **r** is running in the z direction.

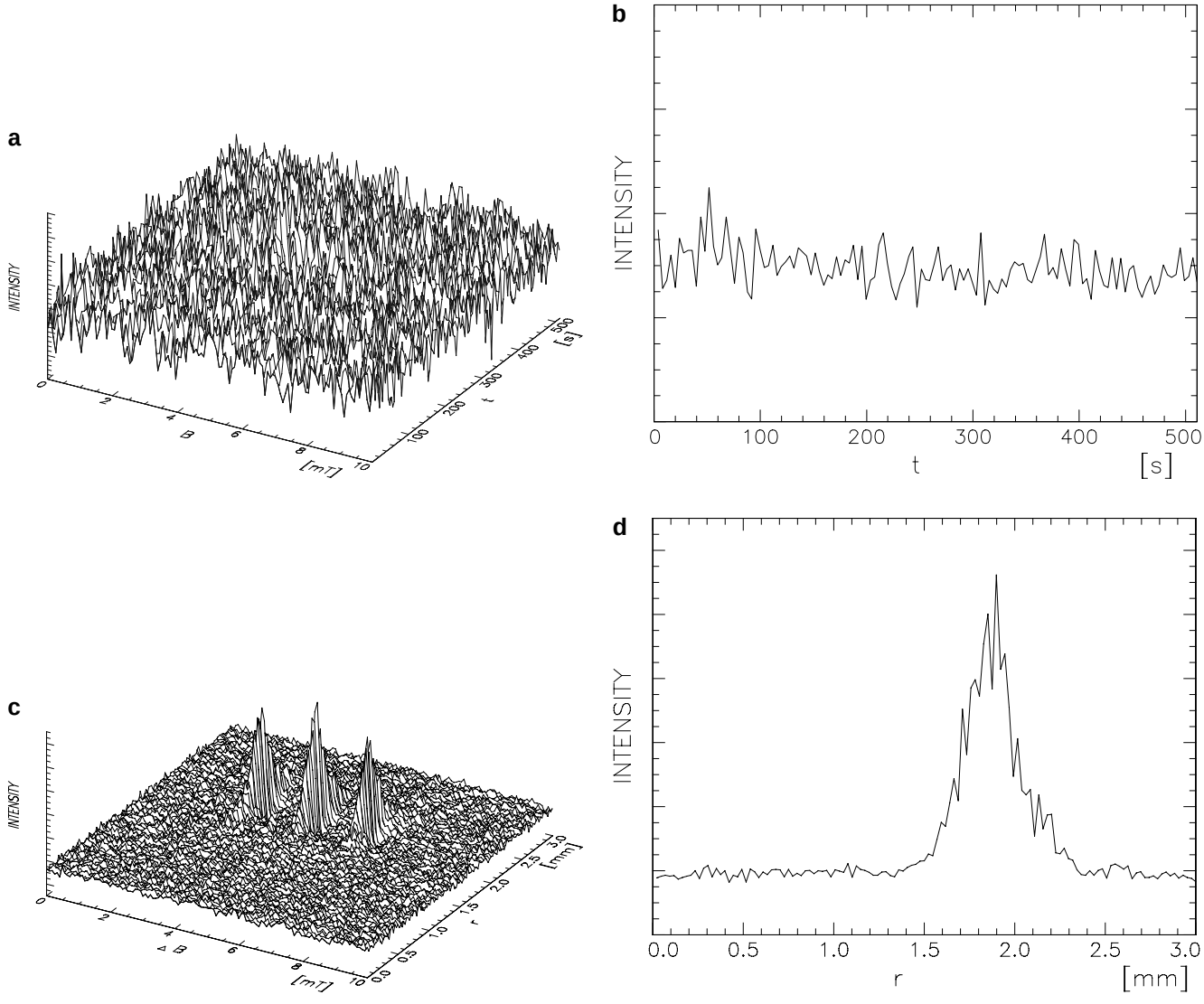

FIG. 3. (a) Localized 2D spectral–temporal image IM(**B**, t)$_{ro}$ measured in a zero-plane at $\mathbf{r}_o$ of the lower dermis during a period of 512 s with a time interval of 4 s between two successive spectra. A spectral scan range of 10 mT was used for a magnetic midfield of $B_0 = 330$ mT. The surface of the skin was constantly in contact with the spin probe Tempol (1 mM) mixed in a microemulsion and contained in the reservoir of the tissue cell. (b) 1D temporal image IM(t)$_{Bo,ro}$ of Fig. 3a which corresponds to the magnitude of the midfield peak versus time for a period of 512 s. No penetration of Tempol in the lower dermis can be seen. (c) Timed 2D spectral–spatial image IM(**B**, **r**)$_{to}$ of the skin biopsy measured after the spectral–temporal image in Fig. 3b. Thus, the total time interval was 1024 s. Although the spin probe Tempol is applied on the skin surface by the spin probe reservoir for the whole measuring time, no penetration of Tempol in the skin could be seen. The spin probe is only contained in the reservoir. (d) 1D spatial image IM(**r**)$_{Bo,to}$ representing the midfield peak versus the spatial axis **r** and confirming the fact that Tempol is completely contained in the reservoir.

The recording time for a 1D scan and a 2D image depends on the modulation frequency f_m of the field gradient and the corresponding time constant of the signal low pass filter which must fulfill the following condition: $\tau \geq 1/2\, f_m$. Using a modulation frequency $f_m = 70$ Hz, the time constant τ must be $\geq 1/140$ Hz $= 7$ ms. We have chose for these experiments a time constant of $\tau = 20$ ms. This time constant results in a recording time t_p for one spectral or spatial scan with $n_p = 128$ pixel, which amounts to $t_p \geq \tau\, n_p = 0.02\ \text{s} \cdot 128 = 2.56$ s. A scan time of $t_p = 4$ s was adjusted for a spectral scan of 10 mT and a spatial scan of 3 mm. Corresponding to a 2D image matrix (128×128) a recording time of $t_d = 512$ s was necessary. The highest modulation frequency of our experimental arrangement could be $f_m = 180$ Hz, which would result in a recording time of

$$t_d = 1/2\, f_m \cdot n_p^2 = 1/180\ \text{Hz} \cdot (128)^2 = 91\ \text{s}$$

for a 2D image.

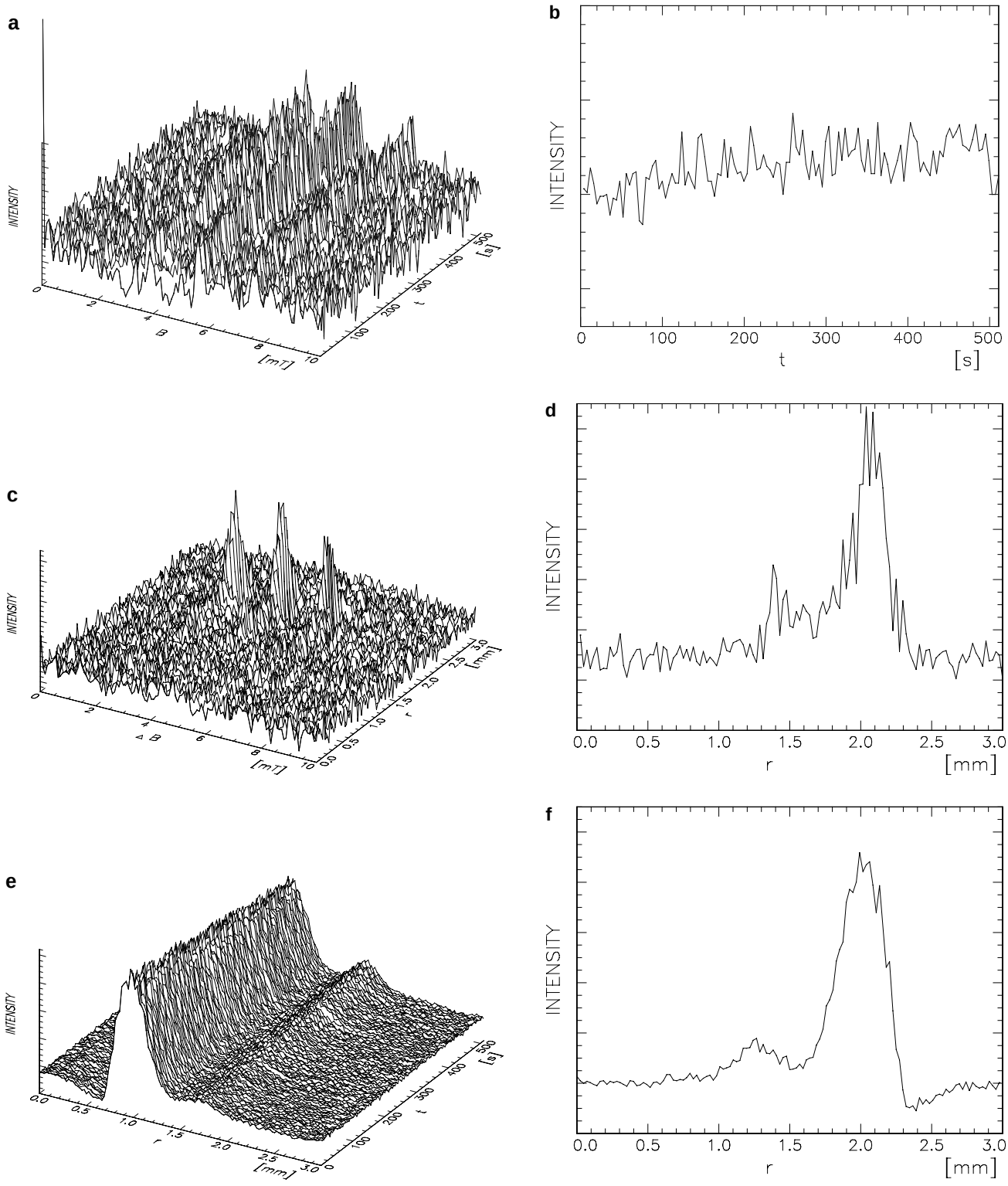

FIG. 4. (a) Localized 2D spectral–temporal image IM(**B**, t)$_{\mathrm{ro}}$ measured in a plane of the lower dermis over a period of 512 s after a chemical treatment with DMSO (30%) for 10 min. Tempol (1 mM) was contained in the reservoir of the tissue cell. The spectral range varied over 10 mT for a midfield $B_0 = 330$ mT. (b) Localized 1D temporal image IM(t)$_{\mathrm{Bo,ro}}$ of Fig. 4a measured at the midfield peak B_0 over a period of 512 s. (c) Timed 2D spectral–spatial image IM(**B**, **r**)$_{\mathrm{to}}$ of the skin biopsy measured after the same period as in Fig. 3c. As can be clearly seen, Tempol has penetrated into the skin. (d) 1D spatial image IM(**r**)$_{\mathrm{Bo,to}}$ representing the magnitude of the midfield peak at B_0 versus the spatial axis z which confirms the fact that Tempol has penetrated into the skin and is enriched in the lower dermis. (e) Field fixed 2D spatio–temporal image IM(**r**, t)$_{\mathrm{Bo}}$ representing the penetration of Tempol into the skin by a sequence of 128 1D profiles measured at regular time intervals of 4 s. The higher signal intensity as compared with other measurements is caused by a higher Tempol concentration of 3 mM in the reservoir. (f) 1D spatial image IM(**r**)$_{\mathrm{Bo,to}}$ of the distribution of Tempol in the skin corresponding to the 15th 1D profile of the 2D image of Fig. 4e representing a distinct enrichment of Tempol in the lower dermis. The spatial profile was measured 116 s after contacting the skin with the Tempol reservoir (60 s preparation time + 56 s measuring time).

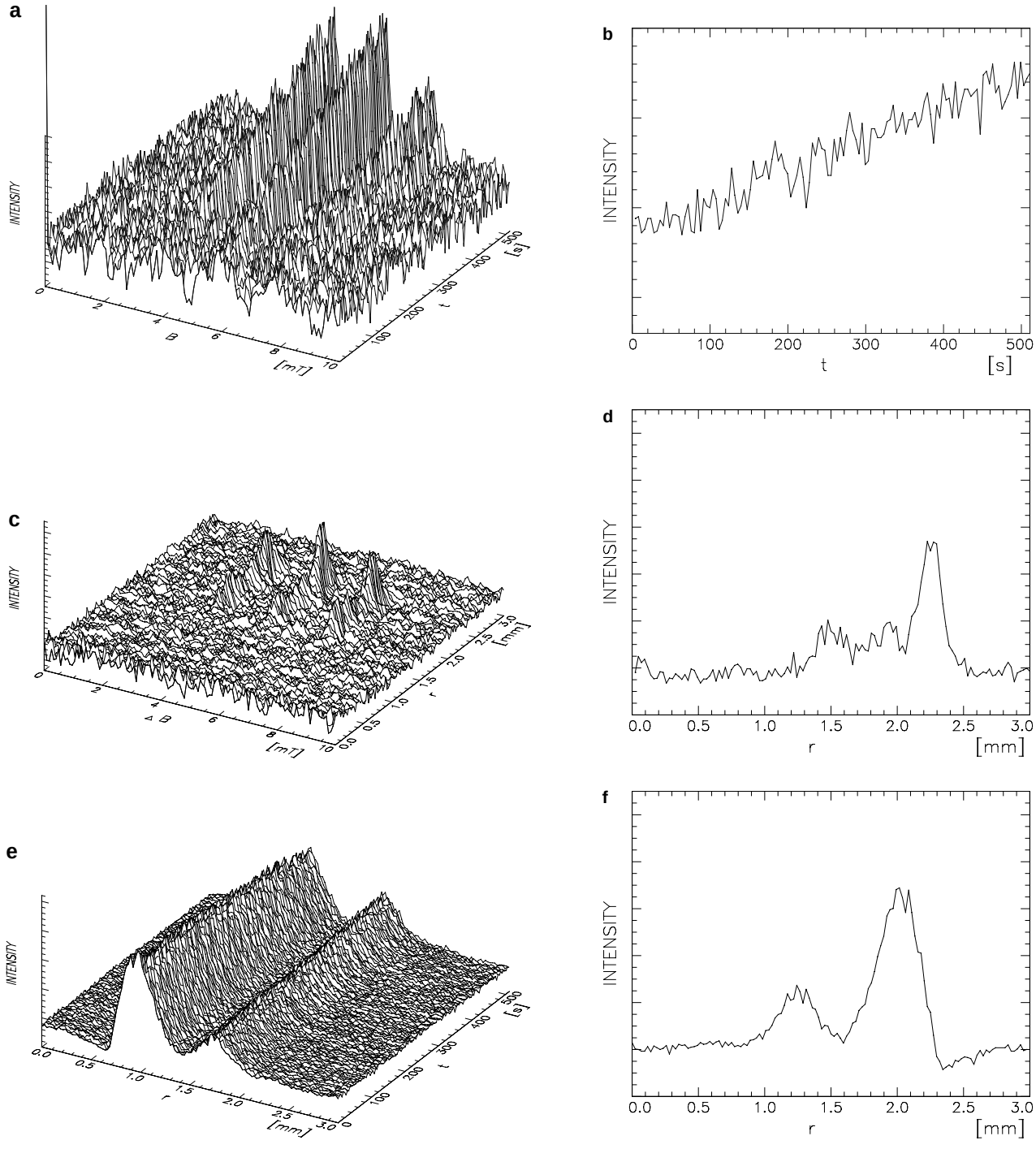

FIG. 5. (a) Localized 2D spectral–temporal image IM(**B**, t)$_{\mathrm{ro}}$ measured in a plane of the lower dermis after removing the horny layer by tape stripping. The skin was permanently treated with an emulsion containing the spin probe Tempol (1 mM) in the tissue cell reservoir. One hundred twenty-eight spectra were measured over a spectral range of 10 mT with a midfield of $B_0 = 330$ mT. The 2D image was measured over a time period of 512 s. (b) Localized 1D temporal image IM(t)$_{\mathrm{Bo,ro}}$ of the midfield $B_0 = 330$ mT of Fig. 5a represents the strong intensity increase in the lower dermis versus a time period of 512 s. (c) Timed 2D spectral–spatial image IM(**B**, **r**)$_{\mathrm{to}}$ of the whole skin biopsy measured after a time period of 512 s (measuring time of the spectral–temporal image). The penetration of Tempol in the skin is clearly seen. One hundred twenty-eight spectra were measured over a spectral range of 10 mT with a mid field of $B_0 = 330$ mT within a time period of 512 s. (d) 1D spatial image IM(**r**)$_{\mathrm{Bo,to}}$ represents the spatial distribution of Tempol in the skin (spatial range of 3 mm) which was measured at the midfield $B_0 = 330$ mT of Fig. 5c. The increase of Tempol in the skin is correlated with a clear decrease in the reservoir. (e) Field fixed 2D spatio–temporal image IM(**r**, t)$_{\mathrm{Bo}}$ consisting of 128 spatial profiles measured in a time period of 512 s that clearly shows the penetration of Tempol in the skin after stripping the horny layer. To enhance the sensitivity the concentration of Tempol was increased up to 3 mM. The image shows clearly the decrease of Tempol in the reservoir and its increase in the lower dermis. Already the first spatial profile shows a distinct peak of Tempol in the lower dermis, which supports the effectiveness of the horny layer as a penetration barrier. (f) 1D spatial profile IM(**r**)$_{\mathrm{Bo,to}}$ of Tempol in the skin which corresponds to the 15th spatial distribution of Fig. 5e. The spatial profile was measured 116 s after contacting the skin with the Tempol reservoir (60 s preparation time + 56 s measuring time). A distinct enrichment of Tempol in the dermis is seen.

RESULTS

Using MOSS imaging, two techniques are available for the detection of fast diffusion processes. With spectral–temporal imaging we measured the appearance of the spin probe Tempol in a lower skin layer to see if and when it overcomes the upper skin barrier, the horny layer. With a time resolution of 4 s 128 spectra at the lower dermis were measured. The 2D spectral–temporal image $\mathrm{IM}(\mathbf{B}, t)_{\mathrm{ro}}$ of the lower dermis in Fig. 3a shows no appearance of Tempol in this layer over a time interval of 512 s. To confirm this fact the cross section through Fig. 3a measured at the midfield peak versus time is represented in Fig. 3b. All represented spectra are normalized to the maximum signal intensity. Both, the 2D image and the 1D cross section show that after the time interval of the measurement of 512 s and a sample preparation time of 60 s no Tempol could reach the lower dermis layer. An overview of the spatial distribution of Tempol in the sample arrangement after that time is shown in Fig. 3c, which demonstrates clearly that Tempol is only situated in the reservoir. A cross section through Fig. 3c represents the amplitude of the midfield peak versus the spatial axis in Fig. 3d. This image confirms the fact that Tempol is only contained in the reservoir. No penetration into the skin could be measured over the observed time interval of the measurement of the two 2D images, which was 1024 s.

An improvement of the penetration of Tempol can be seen after the chemical treatment of the skin with the penetration enhancer DMSO. The 2D image in Fig. 4a and the 1D image in Fig. 4b show that Tempol appears immediately during the first measurement in the lower dermis. The first measurement is delayed by 60 s from the first contact between the reservoir of Tempol and the surface of the skin which was necessary for assembling the tissue cell and mounting it in the cavity. The spatial and spectral distributions of Tempol in the reservoir and the skin are seen in Fig. 4c. The cross section through Fig. 4c is represented in Fig. 4d. It shows the intensity of the midfield peak versus the spatial axis and demonstrates that Tempol penetrated into the skin. It seems that Tempol is enriched in the dermis, contrary to the horny layer and the epidermis. This result seems to be correct because the water content of the epidermis is very low (about 10–20%), contrary to the dermis which is about 70–80%.

The third possibility of the MOSS imaging technique is the measurement of the spatio–temporal images $\mathrm{IM}(\mathbf{r}, t)_{\mathrm{Bo}}$ and was performed with a higher Tempol concentration of 3 mM in the reservoir of the tissue cell.

One hundred twenty-eight spatial distributions $\mathrm{IM}(\mathbf{r})_{t,\mathrm{Bo}}$ of the midfield peak at B_{o} were measured in a time interval of 512 s, which means every 4 s a new spatial distribution was measured. The 128 1D profiles are represented in the spatio–temporal 2D image $\mathrm{IM}(\mathbf{r}, t)_{\mathrm{Bo}}$ in Fig. 4e, which demonstrates the time dependent increase of Tempol in the dermis with a time resolution of 4 s between two measurements. The 1D profile of the 15th measurement, which corresponds to a treatment time of 2 min (inclusive the preparation time of 60 s) of Tempol on the skin, is seen in Fig. 4f. The 2D image and the 1D profile confirm again the fact that Tempol is enriched in the dermis. It is seen that influencing the horny layer by a chemical penetration enhancer like DMSO can result in an immediate increase of Tempol in the dermis.

The mechanical removal of the horny layer by stripping should result in a drastically increased penetration of Tempol into the skin. Figure 5a represents the 2D spectral–temporal image $\mathrm{IM}(\mathbf{B}, t)_{\mathrm{ro}}$ measured in the plane of the lower dermis. A strong increase of Tempol as a function of time is clearly visible. The increase, which corresponds to a linear function, can be seen in Fig. 5b, which represents the cross section through Fig. 5a showing the intensity of the midfield peak versus time with a time resolution of 4 s. The increase is higher compared to the penetration profile in Fig. 4b. A 1-mM Tempol concentration was used for the microemulsion in the reservoir for both measurements. The spectral–spatial measurement of the whole spatial distribution of Tempol in the skin was performed on the same experimental arrangement including the time delay of 512 s for the measurement of the 2D image $\mathrm{IM}(\mathbf{B}, t)_{\mathrm{ro}}$ and the preparation time of 60 s. The 2D spectral–spatial image is seen in Fig. 5c and the 1D spatial profile, which corresponds to the cross section through Fig. 5c showing the intensity of the midfield peak versus the spatial $\mathbf{r}$ axis, is seen in Fig. 5d.

The enrichment of Tempol in the dermis and a corresponding decrease in the reservoir could be distinctly shown in a further measurement using a Tempol concentration of 3 mM. The 2D spatio–temporal image $\mathrm{IM}(\mathbf{r}, t)_{\mathrm{Bo}}$ in Fig. 5e shows an appearance of Tempol already for the first spatial profile. This image demonstrates that after removing the horny layer Tempol can penetrate immediately in the deeper layer of the skin. For analyzing the difference between the chemical and physical treatment of the skin the spatial distribution of the 15th measurement is represented in Fig. 5f. The comparison between Figs. 4f and 5f shows clearly a higher enrichment of Tempol in the dermis after removing the horny layer. This higher enrichment is correlated with a lower concentration of Tempol in the reservoir.

CONCLUSION

The images presented demonstrate the versatility of the MOSS imaging technique for the investigation of diffusion processes. Three different methods result in three different images which describe the diffusion process. The penetration of an aqueous solution of Tempol into the skin was used as the object of demonstration. The skin is a very differentiated model consisting of different layers with different penetration and solubility properties for the spin probe Tempol. The barrier function of the horny layer which works like a membrane and the affinity of the dermis for the Tempol solution could be confirmed very clearly. An applied spatial resolution of $\Delta z = 23\ \mu\mathrm{m}$ is too small for a spatial resolution of the horny layer with a thickness of about 10 μm. But the effect of this thin layer is clearly visible.

The penetration measurements of a spin probe in the skin with the MOSS imaging technique have shown the practical application of the three different methods of the modulated gradient inclusive the rapid field scan. The penetration of water soluble substances into the skin is of great importance especially for the pharmaceutical research. The modulated field gradient technique seems a proper way for such fast diffusion measurements which proceed in the order of some seconds. In comparing the MOSS imaging technique with the normally used spectral–spatial imaging technique with gradient variation, some advantages like higher spatial resolution, higher time resolution, and higher versatility combined with the localized spectroscopy are obvious.

REFERENCES

1. U. Ewert and Th. Herrling, Spectrally resolved tomography with stationary gradient, *Chem. Phys. Lett*. **129,** 516 (1986).
2. M. M. Maltempo, S. S. Eaton, and G. R. Eaton, Spectral-spatial two-dimensional EPR imaging, *J. Magn. Reson*. **72,** 449 (1987).
3. M. M. Maltempo, S. S. Eaton, and G. R. Eaton, Reconstruction of spectral-spatial two-dimensional EPR images from incomplete sets of projections without prior knowledge of the component spectra, *J. Magn. Reson*. **77,** 75 (1988).
4. M. M. Maltempo, S. S. Eaton, and G. R. Eaton, Artifacts in spectral-spatial EPR images of portions of spectra, *J. Magn. Reson*. **85,** 303 (1989).
5. G. R. Eaton, S. S. Eaton, and M. M. Maltempo, Three approaches to spectral-spatial EPR imaging, *Appl. Radiat. Isot*. **40,** 1227 (1989); *Biophys. J*. **59,** 950 (1991).
6. U. Ewert, R. H. Crepeau, C. R. Dunnam, D. Xu, S. Lee, and J. H. Freed, Fourier transform electron spin resonance imaging, *Chem. Phys. Lett.* **184,** 25 (1991).
7. Y.-K. Shin, U. Ewert, D. E. Budil, and J. H. Freed, Microscopic versus macroscopic diffusion in model membranes by electron spin resonance spectral-spatial imaging, *Biophys. J.* **59,** 950 (1991).
8. Y. Morita, K. Ohno, K. Ohashi, and J. Sohma, ESR imaging investigation on depth profiles of radicals in organic solid dosimetry, *Appl. Radiat. Isot.* **40,** 1237 (1989).
9. S. Schlick, J. Pilar, S.-C. Keweon, J. Vacik, Z. Gao, and J. Labsky, Measurements of diffusion processes in HEMA-DEGMA hydrogels by ESR imaging, *Micromolecules* **28,** 5780 (1995).
10. Th. Herrling, N. Klimes, W. Karthe, U. Ewert, and B. Ebert, EPR zeugmatography with modulated magnetic field gradient, *J. Magn. Reson.* **49,** 203 (1982).
11. Th. Herrling, K. A. Thiessenhusen, and U. Ewert, Fast spectral-spatial EPR imaging with modulated gradient and simultaneous field scan, *J. Magn. Reson.* **100,** 123 (1992).
12. Th. Herrling, N. Groth, K.-U. Thiessenhusen, J. Fuchs, and U. Ewert, Spectral-spatial skin imaging with modulated gradient and simultaneous field scan (MOSS), *in* "Magnetic Resonance Microscopy" (B. Blümich and W. Kuhn, Eds.), VCH, Weinheim/New York (1992).
13. J. Fuchs, H. J. Freisleben, N. Groth, Th. Herrling, G. Zimmer, R. Milbradt, and L. Packer, One- and two-dimensional electron paramagnetic resonance imaging in skin, *Free Rad. Res. Commun.* **15,** 245 (1991).
14. J. Fuchs, N. Groth, Th. Herrling, R. Milbradt, G. Zimmer, and L. Packer, Electron paramagnetic resonance (EPR) imaging in skin: Biophysical and biochemical microscopy, *J. Invest. Dermatol*. **98,** 713 (1992).
15. Th. Herrling, N. Groth, and J. Fuchs, Biochemical EPR imaging of skin, *Appl. Magn. Reson.* **11,** 471 (1996).
16. K. Mäder, H.-H. Borchert, R. Stösser, N. Groth, and Th. Herrling, Modelluntersuchungen zur lokalisation und mobilität von arzneistoffen in polymerfolien mit hilfe der ESR-tomographie, *Pharmazie* **46,** 439 (1991).
17. T. Pali, L. Sass, L. I. Horvath, and B. Ebert, 2D ESR image reconstruction from 1D projections using the modulated field gradient method, *J. Magn. Reson.* **86,** 338 (1990).
18. F. Demsar, P. Cevc, and M. Schara, Diffusion of spin probes in tissue measured by field-gradient EPR, *J. Magn. Reson.* **69,** 258 (1986).
19. J. Kristl, S. Pecar, J. Korbar-Smid, F. Demsar, and M. Schara, Drug diffusion: A field gradient electron paramagnetic resonance study, *Drug Develop. Industrial Pharm.* **15,** 1423 (1989).
20. G. Bacic, T. Walczak, F. Demsar, and H. M. Swartz, Electron spin resonance imaging of tissues with lipid-rich areas, *J. Magn. Reson.* **8,** 209 (1988).
21. V. Gabrijelcic, M. Sentjurc, and J. Kristl, Evaluation of liposomes as drug carriers into the skin by one-dimensional EPR imaging, *Int. J. Pharmaceutics* **62,** 75 (1990).
22. J. L. Zweier, G. He, A. Samouilov, P. Kuppusamy, and M. Davies, *In vivo* EPR imaging of human skin: A non-invasive technique to map skin redox metabolism, XXI, IFSCC International Congress 2000 Berlin, abstract PO 3.
23. P. Kuppusamy, M. Chzhan, A. Samouilov, P. Wang, and J. L. Zweier, Mapping the spin-density and lineshape distribution of free radicals using 4D spectral-spatial EPR imaging, *J. Magn. Reson.* **107,** 116 (1995).
24. R. J. Scheuplein and I. Blank, Permeability of the skin, *Phys. Rev.* **51,** 702 (1971).
25. R. Scheuplein, Percutaneous absorption after twenty-five years: Or "old wine in new winwskins," *J. Invest. Dermatol*. **67,** 31 (1976).
26. R. Scheuplein and L. R. Ross, Effects of surfactants and solvents on the permeability of epidermis, *J. Soc. Cosmet. Chem.* **21,** 853 (1970).
27. Y. Kawasaki, D. Quan, K. Sakamoto, R. Cooke, and H. Maibach, Influence of surfactant mixtures on intercellular lipid fluidity and skin barrier function, *Skin Res. Technol.* **5,** 96 (1999).
28. C. L. Gay, T. M. Murphy, J. Hadgraft, I. W. Kellaway, J. C. Evans, and C. C. Rowlands, An electron spin resonance study of skin penetration enhancers, *Int. J. Pharmaceutics* **49,** 39 (1989).
29. J. Mizushhima, Y. Kawasaki, T. Tabohashi, T. Kitano, K. Sakamoto, M. Kawashima, R. Cooke, and H. I. Maibach, Effect of surfactants on human stratum corneum: Electron paramagnetic resonance study, *Int. J. Pharmaceutics* **197,** 193 (2000).
30. H. Wahlquist, Modulation broadening of unsaturated Lorentzian lines, *J. Chem. Phys.* **35,** 1013 (1960).
31. J. A. Weil, J. R. Bolton, and J. E. Wertz, *in* "Electron Paramagnetic Resonance—Elementary Theory and Practical Application," pp. 492–509. Wiley, New York (1994).
32. Th. Herrling, J. Rehberg, F. Klein, and N. Groth, EPR instrumentation for in vivo investigation in human skin, *in* "Modern Applications of EPR/ESR" (C. Z. Rudowicz, K. N. Yu, and Hiroaka, Eds.), pp. 83–87, Springer-Verlag, Singapore (1998).